# Experimental Investigation and Characterization of Innovative Bifacial Silicon Solar Cells

Fabio Ricco Galluzzo[1, 2,*], Luca Zumbo[1, 2],Gianluca Acciari [3], Gabriele Adamo[3], Guido Ala[3], Alessandro Busacca[3], Massimo Caruso[3], Cosimo Gerardi[4], Salvatore Lombardo[1], Rosario Miceli[3], Antonino Parisi[3], Giuseppe Schettino[3] and Fabio Viola[3]

[1] Istituto per la Microelettronica e Microsistemi - Consiglio Nazionale delle Ricerche, Zona Industriale, Ottava Strada n. 5, 95121 Catania, Italy; fabioricco.galluzzo@imm.cnr.it; luca.zumbo@gmail.com; salvatore.lombardo@imm.cnr.it

[2] Dipartimento di Fisica e Astronomia, Università di Catania, Via S. Sofia, 64, 95123 Catania, Italy

[3] Dipartimento di Ingegneria, Università di Palermo, Viale delle Scienze, Ed.9, 90128 Palermo (Italy); gabriele.adamo@unipa.it; antonino.parisi@unipa.it; massimo.caruso16@community.unipa.it; rosario.miceli@unipa.it; claudio.arnone@unipa.it; alessandro.busacca@unipa.it

[4]ENEL Green Power, Contrada Blocco Torrazzesn - Z.I., 95121 Catania, Italy; cosimo.gerardi@enel.com

*Correspondence: fabioricco.galluzzo@imm.cnr.it

‡ Corresponding Author: Fabio Ricco Galluzzo, Ottava Strada n. 5, 95121 Catania, Italy

fabioricco.galluzzo@imm.cnr.it;

*Received: 12.11.2019 Accepted:04.12.2019*

**Abstract-** The interest towards bifacial PV technology has increased over the last years, due to its potential capability of obtaining higher efficiencies with respect to traditional monofacial cells. Thus, the aim of this work is to present an experimental investigation on an innovative photovoltaic technology, such as the bifacial solar cells based on monocrystalline substrate. This analysis is mainly based on the determination of the current density/voltage, power density/voltage, External Quantum Efficiency (EQE) and Laser Beam Induced Current (LBIC) characterization. Interesting results are presented and discussed, demonstrating that the bifacial silicon solar cells can be a very promising technology with high electrical performances and efficiency.

**Keywords** Bifacial solar cells; LBIC; PERT; Electrical characterization.

## 1. Introduction

In recent years, the scientific research in the field of photovoltaic technology has directed the effort towards an innovative concept of solar cells (even if conceived decades ago [1], but not gaining relevant attention), namely bifacial PV systems, capable of overcoming the challenges in terms of efficiency improvement of traditional monofacial cells [2-8]. Indeed, bifacial cells can be illuminated both from the front and rear surfaces, increasing, therefore, the output power with respect to traditional PV systems. This fact is due to the absorption of ground-reflected energy, which depends on both the system configuration and climate [9-11]. Moreover, this new technology allows an optimal adoption of the involved materials [12], increasing also the durability of the module construction [13]. With regards to the market share projection of this new technology, a significant increase is expected by the year 2027 [14,15].

In order to further increase the efficiency by reducing the losses occurring to the system due to soiling, Bhaduri *et al.* proposed a solution based on the vertical mounting of the bifacial modules [16]. Furthermore, the latter technology has bought an increase of average stabilized efficiency [17].

As a matter of fact, among the bifacial solar devices, a prevalent attention has been oriented towards those adopting a mono-crystalline silicon substrate [18], through which it has recently been possible to achieve overall conversion efficiencies of approximately 26% at the R&D stage, by means of cells based on the so-called Heterojunction with

Intrinsic Thin-layer technology [19-22]. Another PV technology, which has been recently used to successfully manufacture Si based bifacial devices, is represented by the bifacial Si *PERT* (acronym of *passivated emitter, rear totally diffused*) solar cells (see their basic structure in [23]), which are the main subject of the present work.

In this context, the aim of this work is to present an experimental characterization on PERT Si bifacial PV cells samples, which is mainly based on the determination of the current density/voltage, power density/voltage, External Quantum Efficiency (EQE) and Laser Beam Induced Current (LBIC) characterization.

The presented work is organized as follows: the description of the test bench for the electrical characterization of the bifacial modules and the related results are described in Section 2, whereas the LBIC measurements and results are reported in Section 3.

## 2. Electrical Characterization: Experimental Setup, Test Methodology and Main Results

Some initial measurements on bifacial PV cells samples, aimed to quantify their EQE and electrical performances, have been carried out at the CNR-IMM Labs, via the experimental setup depicted in Figures 1, 2 and 3. Furthermore, Figure 4 shows a photograph of two of the tested samples.

According to the schematization in Figure 1, the main components of the experimental setup for measuring the electrical characteristics of the samples are listed below:

- a continuous wave solar simulator (model specified in Figure 1), whose light flux is suitably set via a digital exposure controller;
- a thermostatic chuck, equipped with a specimen holder (consisting of a golden plate) and appropriately interfaced with a temperature stabilized vacuum chuck controller;
- a source meter (Keithley 2651A) and a digital multimeter (Keithley 196), linked (by means of an adequate acquisition board) to a computer (on which the LabVIEW 8.2 software was preloaded).

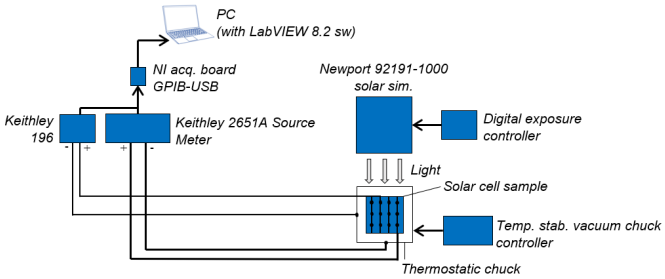


**Fig. 1.** Schematic representation of the experimental setup used to measure the electrical characteristics of the bifacial PV cells samples.

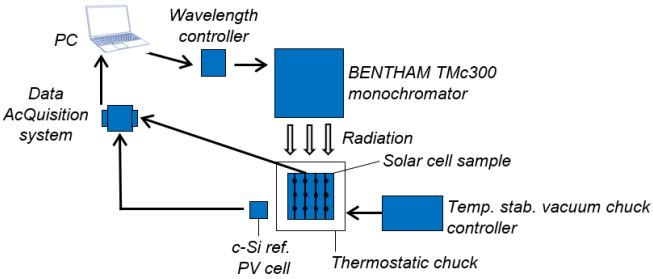


**Fig. 2.** Schematic representation of the experimental setup used to measure the EQE curves of the bifacial PV cells samples.

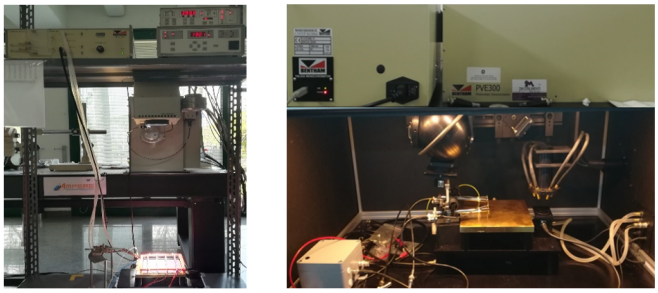

**(a)** **(b)**

**Fig. 3.** Photographs of the experimental setups, available at the CNR-IMM Labs: **(a)** overview of the test bench shown schematically in Figure 1; **(b)** overview of the test bench represented in Figure 2.

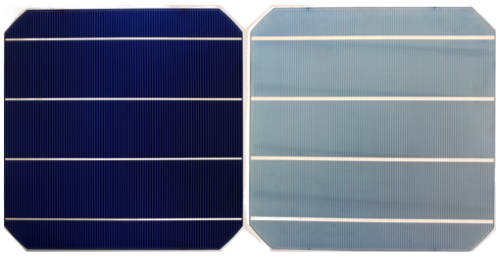

**(a)**

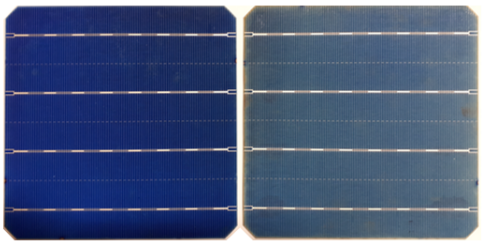

**(b)**

**Fig. 4.** Photographs of two tested samples of bifacial PV cells: **(a)** sample nr. 1; **(b)** sample nr. 2.

By means of such instruments, the electrical characteristics of each sample have been measured. In particular, a suitable 4-wires detection (voltamperometric) system has been adopted, including the abovementioned source meter and digital multimeter. Furthermore, an adequate system of electrodes has allowed to link the bus bars of the PV device under test to the mentioned measurement tools, so that the contact resistance was suitably limited. It has to be noticed that the specimen holder, which consists of a golden plate, has been considered as an electrical potential reference.

According to the schematic of Figure 2, the main devices of the experimental setup used for the EQE measurements are:

- a monochromator (see the model specified in Figure 2);
- a thermostatic chuck with the same characteristics and equipped as already described in the experimental setup of Figure 1;
- a PC (on which BenWin+ software was preloaded), adequately connected to the monochromator through a wavelength controller, in order to scan, acquire (by means of a suitable data acquisition system) and save the responsivity and the EQE trends of the solar cell samples;
- a c-Si reference PV cell, which is used for the calibration of the EQE detection system.

With regards to the experimental methodology used to measure the electrical characteristics of each sample, initially the front side of the device under test was illuminated and subsequently its rear side, under the constant irradiance of 1000 W/m$^2$with AM1.5G spectrum (supplied from the aforementioned solar simulator over the sample surface, orthogonally located to the light beam coming from the simulator) and with a sample temperature maintained constant at 25 °C, through the thermostatic chuck [24,25].

Figure 5 shows the electrical characteristics of the front and rear sides of sample nr. 1, as obtained through the experimental setup previously described (see Figure 1). In particular, Figure 5a shows the current density (J) - voltage (V) curves of the front and rear sides of sample nr. 1 (having a geometric area equal to 235.75 cm$^2$), whereas Figure 5b depicts the power density (dP) – voltage (V) curves of both sides of the same sample. Furthermore, Figure 6 shows the electrical characteristics J-V and dP-V of the front and rear sides of sample nr. 2 (the related geometric area is equal to 241.74 cm$^2$).

Starting from the shown characteristics, the most important electric parameters of a bifacial solar cell, separately referred to its front and rear sides (*i.e.*, the short circuit current density, the open circuit voltage, the series resistance, the maximum power density, related to the PV cell *Maximum Power Point*, the power conversion efficiency and the Fill Factor) can be readily deduced.

As it is easily deduced from Figures 5 (b) and 6 (b), the *bifaciality factor* (defined as the ratio: $\varphi = \frac{\eta_{rear}}{\eta_{front}}$, being $\eta_{rear}$ the cell rear side efficiency and $\eta_{front}$ the cell front side efficiency) of the sample nr. 1 is equal to 0.721, while the bifaciality factor of the sample nr. 2 is approximately 0.832.

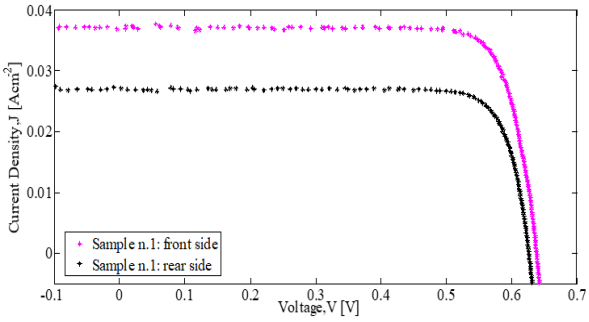


**(a)**

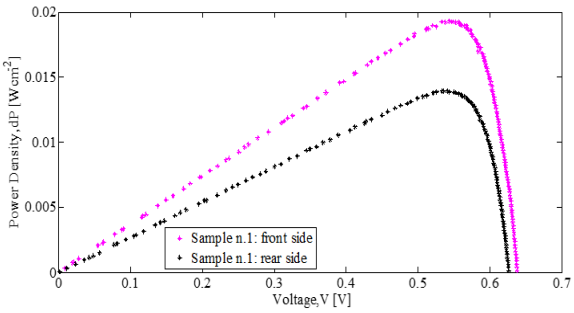


**(b)**

**Fig. 5.** Photographs of two tested samples of bifacial PV cells: **(a)** sample nr. 1; **(b)** sample nr. 2.

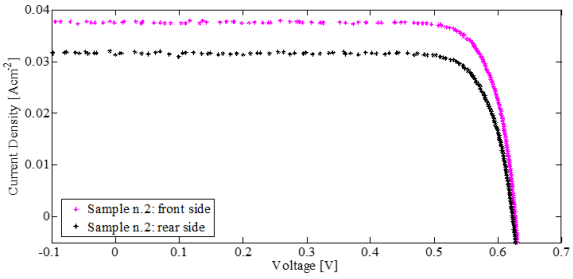


**(a)**

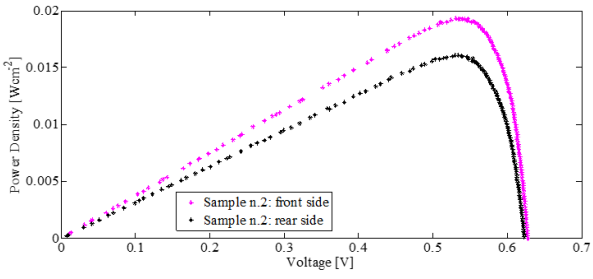


**(b)**

**Figure 6. (a)** J-V and **(b)** dP-V curves of the sample nr. 2 front and rear sides, detected by illuminating the sample at 1000 W/m$^2$ with AM1.5G spectrum and by keeping its temperature at 25 °C.

Figure 7 shows the EQE vs wavelength trends of the front and rear sides of both samples above, obtained through

the experimental setup in Figure 2. From such figure, it is noteworthy that the front side EQE trends of the two samples tested are very similar to each other, instead the ones referring to the rear sides of the same samples seems to be different and this fact could be due to a slightly different metallization of the rear sides of such samples (i.e. a greater metalizationon of the sample nr. 1 rear side, compared to that of the sample nr. 2) which could cause a differnt optic behavior. The previously described results regarding the electrical characterization of the new proposed bifacial cells seem to provide higher performances if compared to other similar works presented in the recent literature [22,26].

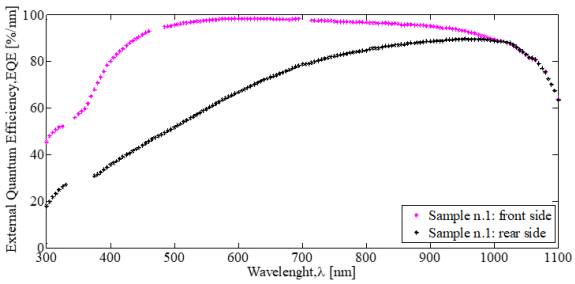


(a)

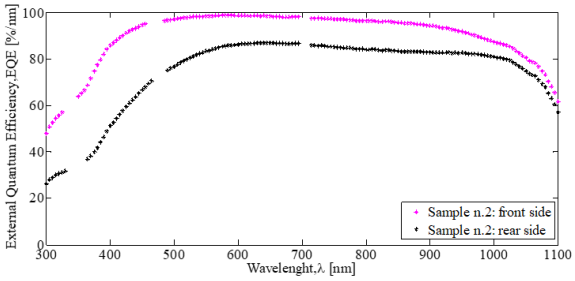


(b)

**Figure 7.** External Quantum Efficiencytrends of front **(a)** and rear **(b)** sides of the two samples tested.

It should be noted that an experimental issue was due to an intrinsic limitation of the experimental setup used, as above illustrated and described. Actually, by illuminating a bifacial solar cell either from its front or its rear side, a reflection of the light transmitted by the solar cell itself occurs, since the above mentioned specimen holder is made of a reflective material (being a golden plate). This fact inevitably affects in some way the measurement of the characteristics.

In order to estimate the effect of using a reflective chuck on the samples short circuit current density values, we carried out further experiments. In particular, for both the above mentioned samples, we have compared the electrical characteristics, measured at the solar simulator in two different experimental configurations, namely by locating each sample: I. over a not reflective black chuck and II. over a copper reflective plate (positioned on the black chuck surface). In both these configurations the 4-wire detection system above descripted was used, by contacting the PV cell via two different electrode systems (one for its front side and one for its rear side). Figure 8 shows the electrical characteristics measured for the two samples tested, at constant irradiance of about 1000 W/m$^2$ and at room temperature. In Table 1 the short circuit current density values are reported for both sides of each sample, as derived from the characteristics shown in Figure 8.

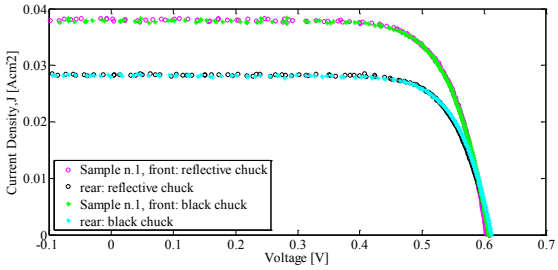


(a)

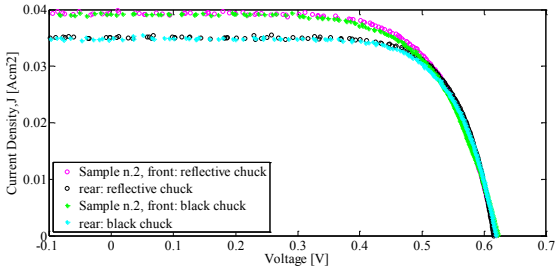


(b)

**Figure 8.** J-V curves of both sides (front and rear) of **(a)** the sample nr.1 and **(b)** the sample nr. 2, at constant irradiance of about 1000 W/m$^2$ with AM1.5G spectrum and at room temperature, by locating the samples alternately over a not reflective black chuck and over a copper reflective plate.

**Table 1.** Short circuit current density (Jsc) values of the samples tested, derived from the characteristics in Figure 8.

| | **Jsc [A/cm$^2$] (reflective chuck)** | **Jsc [A/cm$^2$] (black chuck)** |
|---|---|---|
| **Sample n.1, front** | 0.03807 | 0.03795 |
| **Sample n.1, rear** | 0.02832 | 0.02829 |
| **Sample n.2, front** | 0.03938 | 0.03922 |
| **Sample n.2, rear** | 0.03502 | 0.03485 |

As shown from Table 1, the short circuit current density of both samples tested results very similar in the two experimental configurations considered, but it is noteworthy that the short circuit current density values in the black chuck configuration are lower than those in the reflective chuck

configuration (as it can be easily expected). Hence, in order to rigorously measure in a separate manner the electrical characteristics of the cell front and rear sides, it is advisable to use a specimen holder made of an ideally not reflective material.

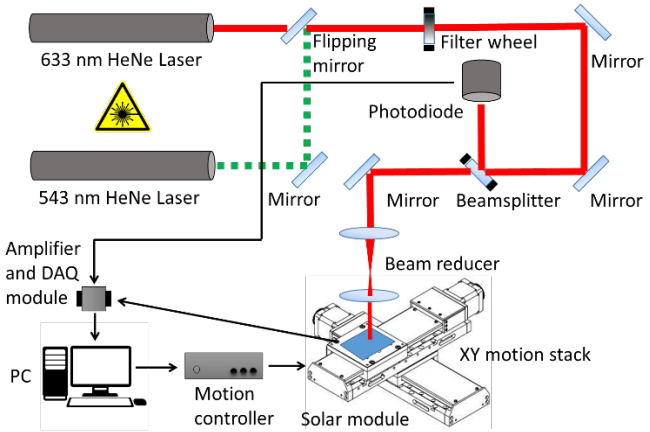


**Figure 9.** Diagram of the LBIC experimental setup.

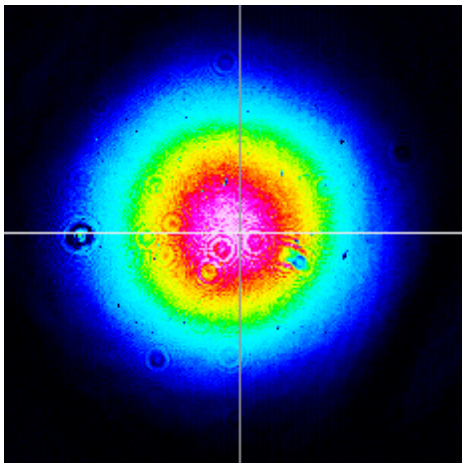

**Figure 10.** The spot shape on the cell as detected by the beam imager. The measured beam diameter is 1.5 mm for the first measurement campaign and 0.22 mm for the second.

## 3. Photoresponse mapping through the LBIC technique

The specimens have been also tested through the Laser Beam Induced Current (LBIC) technique [27-30]. This approach can provide data regarding the photoresponse uniformity of the cell, useful to improve the manufacturing process and highlight discontinuities due to contamination, cracks or degradation. The schematic of the related experimental setup is reported in Figure 9. This characterization was performed at the LOOX Laboratory at the Department of Engineering of the University of Palermo [31,32, 37].

The cells were lighted by employing two continuous HeNe lasers, a red one (632.8 nm, 5 mW) and a green (543.5 nm, 0.5 mW) one, respectively. The emitted optical power was tuned interposing a neutral-density filter wheel between the laser source and the samples.

Considering the long duration of these measurements, even a few tens of hours, the emitted optical power can vary up to 10%. For this reason, it is needed to record the optical power variations that occur during the measurements. This task was accomplished deriving 10% of the emitted optical power to a reference photodiode by means of a beamsplitter.

Moreover, the spot size and the shape on the cell (Figure 10) have been measured by employing a beam imager, thus ensuring that no significant optical aberrations occurred. Furthermore, the choice of the beam diameter, set through a beam reducer, is important being a tradeoff between the spatial resolution of the measurements and their duration. We measured a D4σ beam diameter of 1.5 mm for the first measurement campaign (a 150 x 150 $mm^2$ scan on the entire area of the cell) and of 0.22 mm for the second (a 50 x 50 $mm^2$ scan covering an angle of the cell).

The x-y positioning, on a plane normal to the incident optical beam, is achieved making use of 2 software-controlled linear stages with an accuracy of 5 μm and a maximum excursion of 15 cm along both axes.

The short-circuit photocurrent provided by the cell and the photocurrent delivered by the reference photodiode are pre-amplified and converted into voltage. The two data flows are acquired by two analog inputs of a DAQ module, sampled, and displayed on the PC. The number of measurements per point, the stepper resolution and the scanned area are set via software.

Figure 11 shows the results of the first measurement campaign performed on the sample nr. 1 obtained employing the red HeNe source, 100 acquisitions per point and an incident power density of 1000 $W/m^2$. The same measurements, not reported in this paper, were performed on the sample nr. 2, obtaining almost comparable results. Similar tests were also accomplished, on both the samples, with the green HeNe source but with a lower incident optical power.

Figure 11 exhibits, in 3D surface plots (Figures 11(a) and 11(c)) and 2D contour plots (Figures 11(b) and 11(d)), the output of the tests performed with a step of 1.5 mm between contiguous measurement points on the front and on the back sides of the cell. The front side shows a uniform photoresponse with a maximum variation equal to 4%, while the back side appears less regular with a maximum variation equal to 18%.

In order to investigate in more detail the photoresponse uniformity, we performed further measurements on two corners on the front and back sides of the sample nr. 2, with a higher spatial resolution (0.2 mm step between contiguous measurement points). They are represented in Figs 12 and 13.

These results permit to confirm the previous described outcomes and to appreciate the good uniformity of the photoresponse on the internal edges of the busbars and the fingers and on the external borders, even when compared to other LBIC measurements presented in literature [33-36].

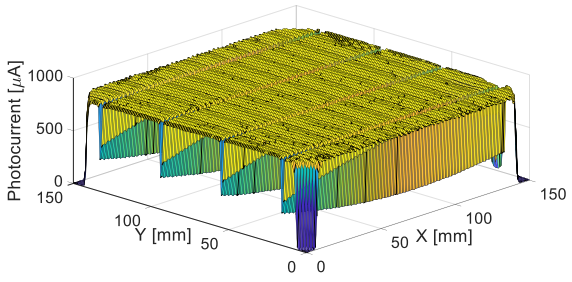


(a)

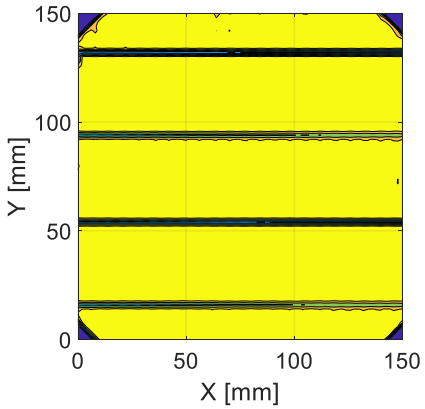


(b)

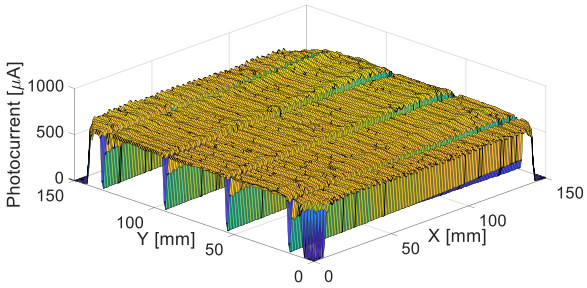


(c)

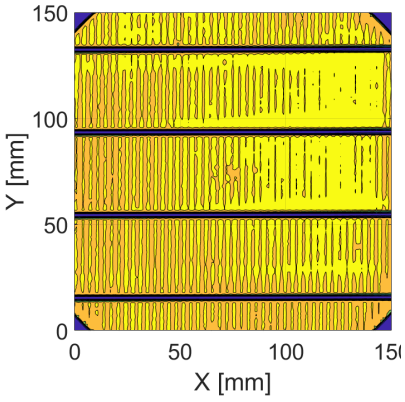


(d)

**Figure 11.** LBIC measurements on sample nr. 1 – **(a)** front side - 3D surface plot **(b)** front side – 2D contour plot **(c)** back side – 3D surface plot **(d)** back side – 2D contour plot.

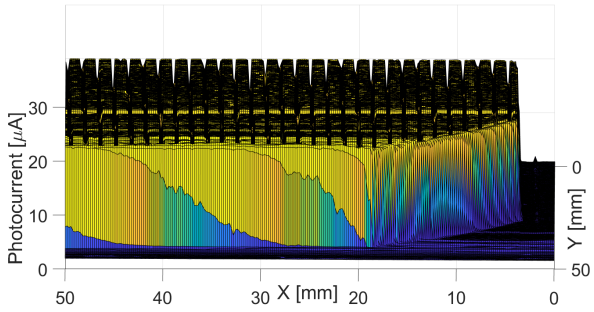


(a)

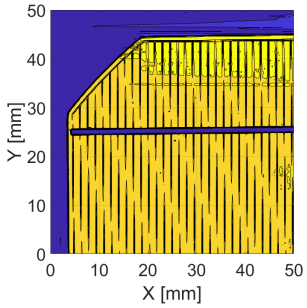


(b)

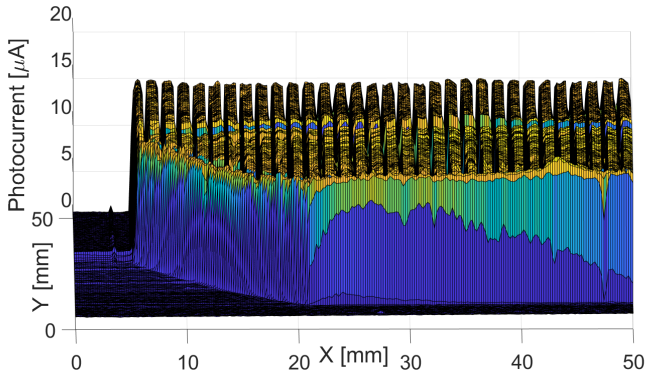


(c)

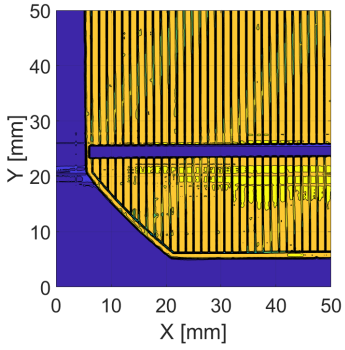


(d)

**Figure 12.** LBIC measurements performed on two corners of the sample nr. 1. Both 3D surface plots and 2D contour plots are provided. **(a)** and **(b)** refer to the front side of the first corner. **(c)** and **(d)** refer to the back side of the first corner.

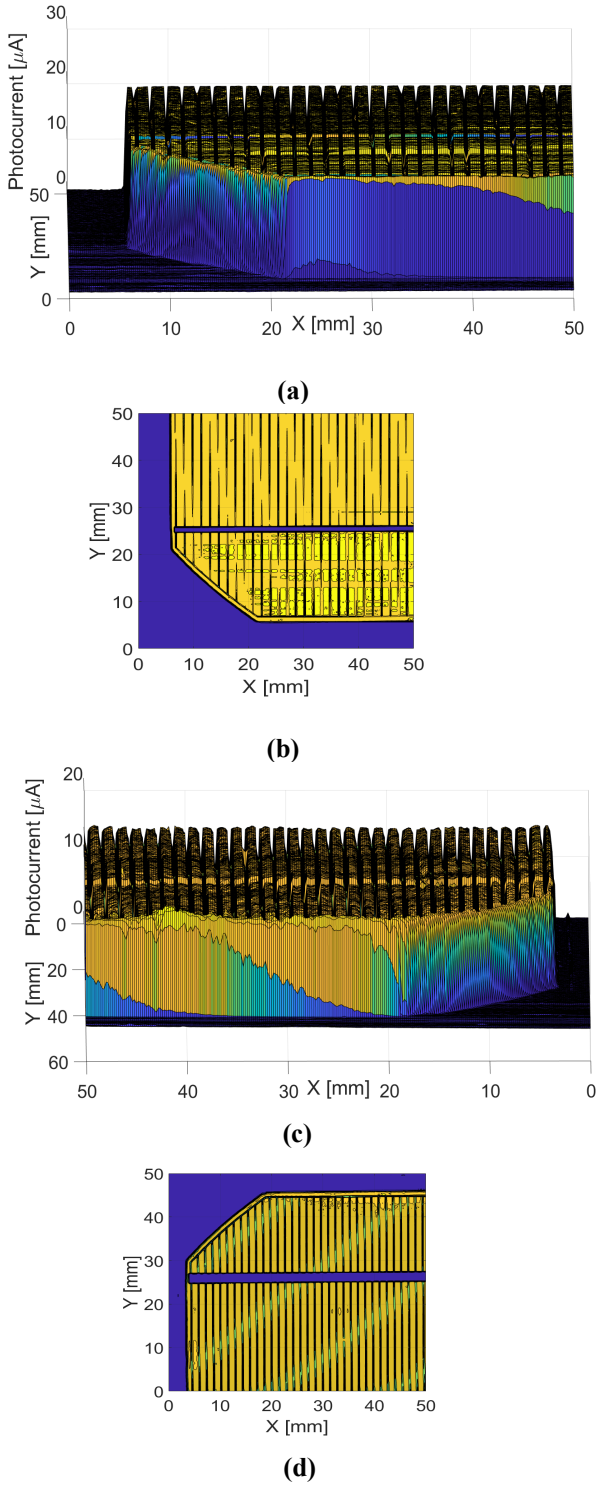


**Figure 13.** LBIC measurements performed on two corners of the sample nr. 1. Both 3D surface plots and 2D contour plots are provided. **(a)** and **(b)** refer to the front side of the second corner. **(c)** and **(d)** refer to the back side.

## 4. Conclusions

This paper has presented an experimental investigation on bifacial silicon solar cells, both in terms of electrical characterization and LBIC analysis.

If compared with traditional PV cells, these results are promising, also considering other similar works in literature. In particular, the LBIC measurements permitted to appreciate the good photoresponse uniformity (employing a minimum measurement step of 0.2 mm), especially on the front side but also on the internal edges (busbars and fingers) and on the external borders.

**Acknowledgments**

The study has been developed from the collaboration between the University of Palermo, ENEL Green Power and the Catania unit of IMM-CNR. The authors kindly thank ENEL Green Power for the provision of the bifacial silicon PV cells.

## References

[1] Hiroshi, M. Radiation energy transducing device. U.S. Patent 3 278 811 A, 1966.

[2] Kopecek, R. et al. Bifaciality: One small step for technology, one giant leap for kWh cost reduction. Photovoltaics Int., 2015, 26, 32–45.

[3] Kerr, M. J.; Cuevas, A.; Campbell, P. Limiting efficiency of crystalline silicon solar cells due to Coulomb-enhanced Auger recombination. Progr. Photovoltaics Res. Appl., 2003, 11, 97–104.

[4] Yalçin, L.; Öztürk, R. Performance comparison of c-Si, mc-Si and a-Si thin film PV by PVsyst simulation. J. Optoelectron. Adv. Mater., 2013, 15, 326–334.
Richter, A.; Hermle, M.; Glunz, S. Crystalline silicon solar cells reassessment of the limiting efficiency for crystalline silicon solar cells. IEEE J. Photovoltaics, 2013, 3, 1184–1191.

[5] Yoshikawa, K.; Yoshida, W.; Irie, T.; Kawasaki, H.; Konishi, K.; Ishibashi, H.; Asatani, T.; Adachi, D.; Kanematsu, M.; Uzu, H.; and Yamamoto, K.; Solar energy materials and solar cells exceeding conversion efficiency of 26% by heterojunction interdigitated back contact solar cell with thin film Si technology. Solar Energy Mater. Solar Cells, 2017, 173, 37–42.

[6] Cuevas, A. The early history of bifacial solar cells. Proc. 20th Eur. Photovolt. Sol. Energy Conf., 2005, 801–805.

[7] Guo, S. Y.; Walsh, T. M.; Peters, M. Vertically mounted bifacial photovoltaic modules: A global analysis. Energy, 2013, 61, 447-454.

[8] Yusufoglu, U. A. et al. Analysis of the annual performance of bifacial modules and optimization methods. IEEE J. Photovolt., 2015, 5, 320–328.

[9] Chieng, Y. K.; Green, M. A. Computer simulation of enhanced output from bifacial photovoltaic modules. Prog. Photovolt., 1993, 1, 293–299.

[10] Kreinin, L. et al. PV module power gain due to bifacial design. Preliminary experimental and simulation data. 35th IEEE Photovolt. Spec. Conf., 2010, 2171–2175.

[11] Ohtsuka, H.; Sakamoto, M.; Tsutsui, K.; Yazawa, Y. Bifacial silicon solar cells with 21·3% front efficiency and 19·8% rear efficiency. Progress in Photovoltaics: Research and Applications. 2000, 8, 385–390.

[12] Jorgensen, G.J.; Terwilliger, K.M.; Kempe, M.D.; McMahon, T.J. Testing of packaging materials for improved PV module reliability. IEEE Phot Spec Conf, 2005, 499-502.

[13] Cellere, G.; Falcon, T. et al. International Technology Roadmap for Photovoltaic (ITRPV), 2016.

[14] Pelaez, S. A.; Deline, C.; MacAlpine, S. M.; Marion, B.; Stein, J. S.; Kostuk, R. K. Comparison of Bifacial Solar Irradiance Model Predictions With Field Validation. IEEE Journal of Photovoltaics, 2019.

[15] Bhaduri, S.; Kottantharayil, A. Mitigation of Soiling by Vertical Mounting of Bifacial Modules. IEEE Journal of Photovoltaics, 2019, 9, 240-244.

[16] Lin, J.; Ho, K.; Haga, S. W.; Chen, W. Symmetrical and Crossed Double-Sided Passivation Emitter and Surface Field Solar Cells for Bifacial Applications. IEEE Journal of the Electron Devices Society, 2019.

[17] Guerrero-Lemus, R.; Vega, R.; Kim, T.; Kimm, A.; Shephard, L. E. Bifacial solar photovoltaics – A technology review. Renewable and Sustainable Energy Reviews, 2016, vol. 60, pp. 1533–1549.

[18] Yoshikawa, K.; Kawasaki, H.; Yoshida, W.; Irie, T.; Konishi, K.; Nakano, K.; Uto, T.; Adachi, D.; Kanematsu, M.; Uzu, H.; Yamamoto, K. Silicon heterojunction solar cell with interdigitated back contacts for a photoconversion efficiency over 26%. Nature Energy, Mar. 2017, vol. 2, p. 17032.

[19] Lin, J. T.; Lee, C. T.; Chen, W. H.; Haga, S. W.; Hu, Y. Y.; Ho, K. Y. Double-Sided Symmetrical and Crossed Emitter Crystalline Silicon Solar Cells With Heterojunctions for Bifacial Applications. IEEE Journal of Photovoltaics, 2018, 8, 441-447.

[20] Campa, A.; Valla, A.; Brecl, K.; Smole, F.; Muñoz, D.; Topic, M. Multiscale Modeling and Back Contact Design of Bifacial Silicon Heterojunction Solar Cells. IEEE Journal of Photovoltaics, 2018, 8, 89-95.

[21] Taguchi, M. et al. 24.7% Record Efficiency HIT Solar Cell on Thin Silicon Wafer. IEEE Journal of Photovoltaics, 2014, 4, 96-99.

[22] Fertig, F.; Nold, S. ; Wöhrle, N. ; Greulich, J.; Hädrich, I.; Krauß, K. ; Mittag, M. ; Biro, D. ; Rein, S. ; Preu, R. Economic feasibility of bifacial silicon solar cells. Prog. Photovolt: Res. Appl., 2016, 24: 800– 817. doi: 10.1002/pip.2730.

[23] Laudani, A.; Riganti Fulginei, F.; Salvini, A.; Parisi, A.; Pernice, R.; Ricco Galluzzo, F.; Cino, A. C.; Busacca, A. C. One diode circuital model of light soaking phenomena in Dye-Sensitized Solar Cells. Optik, 2018, 156, 311-317.

[24] Parisi, A.; Pernice, R.; Adamo, G.; Miceli, R.; Cino, A. C. Anomalous performance enhancement effects in Ruthenium-based Dye Sensitized Solar Cells. ICCEP 2017, 2017, 8004811, 174-178.

[25] Duran, C. "Bifacial Solar Cells: High Efficiency Design, Characterization, Modules and Applications", Konstanzer Online-Publikations-System (KOPS), 2012

[26] Ibrahim, A. LBIC Measurements Scan as a Diagnostic Tool for Silicon Solar Cell. J. Basic. Appl. Sci. Res., 2011, 1, 215-221.

[27] Sites J. et al. Physical Characterization of Thin-film Solar Cells. Prog. Photovolt: Res. Appl., 2004, 12.

[28] Photoresponse Mapping of Photovoltaic Cells, Application note 40, Newport.

[29] Martin, J.; Fernandez-Lorenzo, C.; Poce-Fatou, J. A.; Alcantara, R. A Versatile Computer-controlled Highresolution LBIC System. Prog. Photovolt: Res. Appl., 2004, 12, 283-295.

[30] Adamo, G.; Parisi, A.; Pernice, R.; Ricco Galluzzo, F.; Di Noia, L.; Cino, A. C. Laser Beam Induced Current measurements on Dye Sensitized Solar Cells and thin film CIG(S,SE)2modules. ICCEP 2017, 2017, 169-173.

[31] Parisi, A.; Pernice, R.; Andò, A.; Adamo, G.; Cino, A. C.; Busacca, A. C. Experimental characterization of Ruthenium-based Dye Sensitized Solar Cells and study of light-soaking effect impact on performance. 2016 AEIT International Annual Conference, 2016, 1-5.

[32] Ibrahim, A. LBIC Measurements Scan as a Diagnostic Tool for Silicon Solar Cell. J. Basic. Appl. Sci. Res., 2011, 215-221.

[33] Bokalič, M.; Jankovec, M.; Topič, M. Solar Cell Efficiency Mapping by LBIC. 45th Int. Conf. on Microelectr., Dev. and Mat., 2009, 269-273.

[34] Bezuidenhout, L. J.; van Dyk, E. E.; Vorster, F. J.; du Plessis, M. C. On the Characterisation of solar cells using light beam induced current measurements. In Nelson Mandela Metropolitan University, Centre for Energy Research, Student Symposium, 2012.

[35] Finn, J. R.; Hansen, B. R.; Granata, J. E. Multiple junction cell characterization using the LBIC method: early results, issues, and pathways to improvement. In 2009 34th IEEE Photovoltaic Specialists Conference (PVSC), June 2009, 000564-000569.

[36] Acciari, G.; Adamo, G.; Ala, G.; Busacca, A.; Caruso, M.; Giglia, G.; Imburgia, A.; Livreri, P.; Miceli, R.; Parisi, A.; Pellitteri, F.; Pernice, R.; Romano, P.; Schettino, G.; Viola, F. Experimental Investigation on the Performances of Innovative PV Vertical Structures. *Photonics* 2019, *6*, 86.